

Article

Evaluation of Electromagnetic Exposure of the Human with a Coronary Stent Implant from an Electric Vehicle Wireless Power Transfer Device

Tianhao Wang¹, Bo Li¹ , Kaifeng Zhao¹, Quanyi Yu¹, Linlin Xu¹, Yaodan Chi² and Shanshan Guan^{1,*}

¹ The College of Instrumentation and Electrical Engineering, Jilin University, Changchun 130026, China; wangtianhao@jlu.edu.cn (T.W.); libo21@mails.jlu.edu.cn (B.L.); zhaokf23@mails.jlu.edu.cn (K.Z.); qyyu20@mails.jlu.edu.cn (Q.Y.); xull@mails.jlu.edu.cn (L.X.)

² Jilin Provincial Key Laboratory of Architectural Electricity and Comprehensive Energy Saving, Jilin Jianzhu University, Changchun 130118, China; chiyaodan@jlju.edu.cn

* Correspondence: guanshanshan@jlu.edu.cn

Abstract: The aim of this paper is to analyze in depth the coupling between leakage electromagnetic fields (EMFs) generated by an electric vehicle wireless power transfer (EV-WPT) device under misaligned operating conditions and metallic coronary stents, which could be potentially hazardous to human electromagnetic safety. In this paper, we established that a standing human with a coronary stent implant and a sitting human with a coronary stent implant are exposed to the leaked EMFs of an EV-WPT device with a transmission power of 11 kW and 22 kW and a transmission frequency of 85 kHz, and we quantified the induced *E*-field strength of the human body by considering the *x*- and *z*-axis misalignment ranges of the WPT device as [−75 mm, 75 mm]. The results showed that the enhancement of the induced *E*-field in the human tissues near the sharp edges of the implant is significant. Meanwhile, the larger the WPT device misalignment generated, the higher the transmission power, and the closer the human body is to the WPT device, the larger the induced *E*-field_{max} value of the human body is, which has the possibility of exceeding the ICNIRP safety limit, and there is a potential human body electromagnetic safety problem.

Keywords: electric vehicle (EV); wireless power transfer (WPT); precision medical implants; induced electric field strength; electromagnetic field exposure



Citation: Wang, T.; Li, B.; Zhao, K.; Yu, Q.; Xu, L.; Chi, Y.; Guan, S. Evaluation of Electromagnetic Exposure of the Human with a Coronary Stent Implant from an Electric Vehicle Wireless Power Transfer Device. *Electronics* **2023**, *12*, 4231. <https://doi.org/10.3390/electronics12204231>

Academic Editor: Carlo Petrarca

Received: 1 September 2023

Revised: 21 September 2023

Accepted: 10 October 2023

Published: 13 October 2023



Copyright: © 2023 by the authors. Licensee MDPI, Basel, Switzerland. This article is an open access article distributed under the terms and conditions of the Creative Commons Attribution (CC BY) license (<https://creativecommons.org/licenses/by/4.0/>).

1. Introduction

In recent years, the emergence of electric vehicles (EVs) has eased the pressure of environmental pollution caused by the exhaust of conventional fuel vehicles and dependence on fossil fuels. To improve the safety, reliability, and convenience of EV charging [1,2], various research teams have been working on wireless power transfer (WPT) technologies [3,4]. High-performance WPT devices are required to meet the needs of consumers and commercial users in the EV market [5,6]. The EV-WPT systems with a transmission power of 30 kW at a transmission frequency of 20 kHz and a transmission power of 52 kW at a transmission frequency of 40 kHz were established [7,8]; however, leaked electromagnetic fields (EMFs) of uneven strength are generated around high-power EV-WPT devices, and human electromagnetic safety when exposed to leaked EMFs from these high-power devices needs to be evaluated [9,10]. For leaked EMFs at different frequencies, the International Commission on Non-Ionizing Radiation Protection (ICNIRP) is concerned with different indicators when the frequency is less than 100 kHz to prevent the human nerve stimulation effects considering induced electric field intensity (induced *E*-field) [11]; when the frequency is higher than 100 kHz, the specific absorption rate (SAR) is considered to prevent the local temperature increase in human tissues [12]. The high-power leakage of electromagnetic radiation (EMR) generated by the EV-WPT device impacts molecular ions and electrons, as well as reactive

oxygen species, protein, and DNA/RNA levels. Furthermore, the EMR has cytotoxic effects on cells by causing degeneration, apoptosis, and necrosis. EMR has a substantial impact on the central nervous system, reproductive system, cardiovascular system, and hematological system. Biological systems that are continuously exposed to electromagnetic radiation over a long period of time may experience an increase in tissue temperature [13]. Therefore, this paper performs a quantitative assessment of the induced E -field of the human body exposed to a high-power, 85 kHz transmission frequency EV-WPT device to determine human electromagnetic safety.

The electromagnetic safety of the surrounding human body during the operation of EV-WPT devices has been extensively studied. For example, [14] quantified the induced E -field value of the human body for an EV-WPT device with a transmission power of 7 kW and a transmission frequency of 85 kHz in an electromagnetic exposure environment, considering the WPT device misalignments generated and adult human models in different postures. The author of [15] quantified the induced E -field value of the human body and the safety distance under EV-WPT devices with a transmission frequency of 85 kHz and different transmission powers. The heart is one of the most essential organs in the human body, and its main role is to drive blood flow, deliver oxygen and nutrients to all organs and tissues of the body, and carry away metabolites. However, cardiovascular diseases cause one-third of all deaths annually and are expected to account for 24 million cases by 2030 [16]. Coronary artery stenosis often complicates coronary artery disease and leads to myocardial infarction. Coronary stents are metal mesh tubular structures that are permanently implanted into narrowed arteries to improve the arteries and restore blood supply to the heart [17]. Existing studies have shown that when a human body with a metallic medical implant is placed under an EMF, the implant has the potential to alter the EMF distribution and absorb electromagnetic energy that is absorbed by local tissues and organs of the body, leading to a significant increase in electromagnetic exposure indicators in the vicinity of the implant and the risk of damage to human tissues [18].

There are also a small number of studies related to the quantification of electromagnetic exposure of a human body containing implants under the leaked EMFs of WPT devices. In [19], a quantitative assessment of the SAR of a human body under the leaked EMF of a small radiofrequency WPT antenna implant device at the transmission frequency of 1470 MHz was performed. In [20], the induced E -field value of the human body was studied considering the transmission frequency of 85 kHz and the leaked EMF of EV-WPT devices with different transmission powers on human bodies containing implants such as tibial intramedullary nails and hip joints. In [21], the SAR values of the surrounding human tissues were quantitatively evaluated using an EV-WPT system with a transmission frequency of 13.56 MHz and a transmission power of 5.3 kW, considering implants such as nerve stimulators, hip joints, etc. However, there are fewer studies on the human electromagnetic safety of precision implants, such as those containing coronary stents. In view of the fact that coronary stent implants often have tips and sharp edges, human tissues located in the vicinity of tips and sharp edges of implants under EMFs have higher values of electromagnetic exposure indicators, which may affect the normal physiological function of the heart. At the same time, due to the Society of Automotive Engineers (SAE) standard, there will be a coil offset in the actual operation of the WPT device [22]. When the coil is misaligned, it will generate unevenly distributed leaked EMFs in space, affecting the internal EMF distribution of the human body containing the implant. Therefore, it is important to consider the leaked EMFs of EV-WPT devices for different operating conditions to quantify the electromagnetic exposure of human bodies containing coronary stent implants.

The purpose of this paper is to analyze the electromagnetic safety of humans with coronary stent implants in the vicinity of EV-WPT devices. The electromagnetic exposure of an EV-WPT device with a transmission frequency of 85 kHz and transmission powers of 11 kW [5] and 22 kW [23] and a human body with a coronary stent implantation are modeled. Under the leakage EMFs of the EV-WPT device, the induced E -field of the human

body implanted with a coronary stent is quantified using the magnetic quasi-static (MQS) approach, taking into account the different locations of the human body in the inside and at the rear of the vehicle and the misalignment generated by the WPT device. The rest of this paper is as follows: Section 2 establishes the numerical simulation model of a human containing a coronary stent implant under the electromagnetic exposure of a leaked EMF of an EV-WPT device and introduces the numerical simulation method of human electromagnetic exposure adopted in this paper. Section 3 discusses the different electromagnetic exposure scenarios for the EV-WPT device considered in this paper and quantifies the induced E -field in different postures of the human body containing a coronary stent implant under electromagnetic exposure scenarios. Finally, Section 4 concludes the paper.

2. Models and Methods

2.1. Electromagnetic Numerical Simulation Model of EV-WPT Device

The EV-WPT device used in this paper consists of an EV, a transmitter, and a receiver. As shown in Figure 1a, the main view of the relative position diagram of the established human–vehicle model, the EV in this paper is based on the actual car geometry, and its geometry is $4000 \times 2000 \times 1500$ mm (length \times width \times height), which is close to the geometry of commercial EVs in the market and can be used as a model for the numerical simulation of the EV in this paper. Considering the accuracy of the numerical simulation, the metallic material of the EV body is aluminum, the non-metallic material of the tire is rubber, and the non-metallic material of the glass is tempered glass. As shown in Figure 1b,c, the geometric schematic and misalignment schematic of the WPT device established in this paper are shown. In this paper, the WPT device is based on magnetic resonance technology using a double coil resonance structure, the coil is shaped as a disc, the coil is made of copper metal material, the transmitting coil (TC) and the receiving coil (RC) have the same size, the outer radius is 325 mm, the inner radius is 141 mm, the wire diameter is 2 mm, and the number of turns is 12. To ensure less EMF leakage, a square ferrite shield is used, and the shield dimensions are $650 \times 650 \times 10$ mm (length \times width \times height). Furthermore, in this paper, the relative magnetic permeability of the ferrite material is 2500, and the electrical conductivity is negligible. Based on the real charging scenario of the EV-WPT device, the WPT devices TC and RC are allowed to have bit errors, the initial values of their bit error quantities x_0 and z_0 are set to be 0 mm initially, the distance y_0 between TC and RC is 200 mm, and the WPT device is placed under the rear of the EV (directly underneath the trunk). Considering the electromagnetic exposure of the EV-WPT device to the driver inside the vehicle and pedestrians near the vehicle body during the actual charging, this paper considers the sitting human body located in the driver's seat (2330 mm from the center of the WPT) and the standing human body located at the rear of the vehicle (800 mm from the center of the WPT), respectively. The above completes the establishment of an electromagnetic numerical simulation model of the EV-WPT device.

In this paper, considering the resonant energy transfer with high efficiency of the dual inductor–capacitor–capacitor (LCC) compensation topology network structure [24], the WPT device uses a dual LCC compensation structure. If the WPT device does not include shields, the circuit at this point can be equated to a linear circuit diagram, as shown in Figure 2, with the circuit analyzed as follows. In the dual LCC compensation topology network circuit, I_0 is the excitation source; U_1 is the voltage at the TC end; L_{s1} and R_{s1} are the additional resonance inductance and internal resistance at the TC end, respectively; C_{p1} and C_{s1} are the resonance compensation capacitor and the isolation capacitor at the TC end, respectively; R_1 is the equivalent resistance at the TC end; L_1 is the coil self-inductance at the TC end; M is the coil mutual inductance between TC and RC; L_2 is the coil self-inductance at the RC end; R_2 is the equivalent resistance at the RC end, C_{p2} and C_{s2} are the resonance compensation capacitor and the isolation capacitor at the RC end; L_{s2} and R_{s2} are the additional resonance inductance and the internal resistance at the RC end, respectively; R_L is the load resistance; and U_2 is the voltage at the RC end.

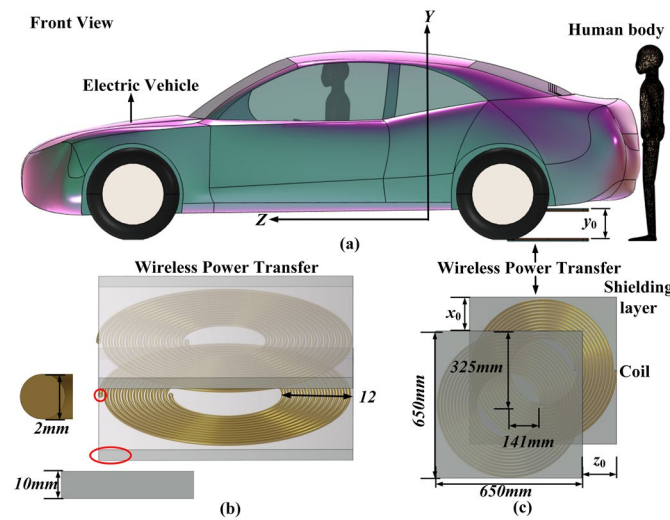


Figure 1. Relative human–vehicle position diagram in EV-WPT device charging scenario. (a) Main view; (b) WPT device geometry model; (c) WPT device misalignment schematic.

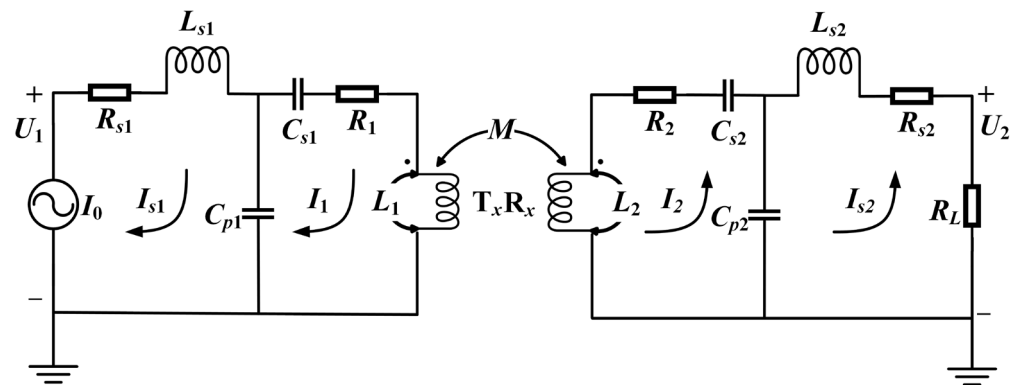


Figure 2. LCC compensation circuit model of WPT device.

The resonance condition at the TC end:

$$\omega L_1 - \frac{1}{\omega C_{s1}} = \frac{1}{\omega C_{p1}} = \omega L_{s1} \tag{1}$$

The resonance condition at the RC end:

$$\omega L_2 - \frac{1}{\omega C_{s2}} = \frac{1}{\omega C_{p2}} = \omega L_{s2} \tag{2}$$

where ω is the resonance angular frequency with the value of $2\pi f$ and f is the resonance frequency.

The loop equations are:

$$\begin{cases} \dot{U}_1 = (R_{s1} + j\omega L_{s1})\dot{I}_{s1} + (R_1 + j\omega L_1 + \frac{1}{j\omega C_{s1}})\dot{I}_1 + j\omega M\dot{I}_2 \\ (R_1 + j\omega L_1 + \frac{1}{j\omega C_{s1}})\dot{I}_1 + j\omega M\dot{I}_2 = \frac{1}{j\omega C_{p1}}(\dot{I}_{s1} - \dot{I}_1) \\ \dot{U}_2 = (R_2 + j\omega L_2 + \frac{1}{j\omega C_{s2}})\dot{I}_2 + (R_{s2} + j\omega L_{s2})\dot{I}_{s2} + j\omega M\dot{I}_1 \\ (R_2 + j\omega L_2 + \frac{1}{j\omega C_{s2}})\dot{I}_2 + j\omega M\dot{I}_1 = \frac{1}{j\omega C_{p2}}(\dot{I}_{s2} - \dot{I}_2) \\ \dot{I}_0 = \dot{I}_1 \\ \dot{U}_2 + \dot{I}_{s2}R_L = 0 \end{cases} \tag{3}$$

The current transfer ratio and voltage transfer ratio are obtained by solving Equations (1) and (2) as shown in Equations (4) and (5):

$$\frac{\dot{U}_2}{\dot{U}_1} = \frac{MR_L}{j\omega L_1 L_2} \quad (4)$$

$$\frac{\dot{I}_{s2}}{\dot{I}_{s1}} = \frac{j\omega L_1 L_2}{MR_L} \quad (5)$$

Continue solving to obtain the transmitter input resistance R_{in} as:

$$R_{in} = \frac{\omega^2 L_1^2 L_2^2}{M^2 R_L} \quad (6)$$

The transmitted power of the EV-WPT device is:

$$P = \left| \operatorname{Re} \left[\dot{U}_1 \dot{I}_{s1}^* \right] \right| = \frac{M U_1 U_2}{\omega L_1 L_2} |\sin \theta| \quad (7)$$

where θ is the impedance angle of U_1 and U_2 , and the maximum power will be reached when the U_2 angle lags behind the U_1 forward transmission, i.e., $\theta = 90^\circ$. In this paper, the EV-WPT device with 22 kW transmission power has a U_1 voltage level of 750 V and a U_2 voltage level of 711.5 V. The EV-WPT device with 11 kW transmission power has a U_1 voltage level of 550 V and a U_2 voltage level of 521.8 V.

2.2. Human Body and Implant Model

In this paper, the whole human body and heart organ models for numerical simulation calculation were constructed using CT scan data with reference to an actual 1750 mm, 75 kg, 30-year-old adult male human body. Considering the diversity of human postures, Figure 3a,c show the standing and sitting adult male human bodies built in this paper, respectively. The numerical simulations in this paper were computed at a frequency of 85 kHz. Most of the electrical properties of the human body are obtained using magnetic resonance imaging [25]. The electromagnetic parameters of the human tissues involved at this frequency are shown in Table 1 [20,26]. The corresponding various human tissues and organs are linearly isotropic homogeneous media. In order to achieve a smooth coronary artery official lumen in the human heart, maintain a low restenosis rate, and make the mechanical properties of the atherosclerotic vessel wall more stable, the structure of the coronary stent considered by numerical simulation in this paper is shown in Figure 4. The coronary stent consists of 24 identical units, each unit consisting of a rectangular ring and two open struts, and the dimensions of the coronary stent are the following: nominal length 19 mm and nominal outer diameter 2.25 mm. Due to the properties of titanium alloy, such as biocompatibility and corrosion resistance, it is widely used in human medical implants [27], so a nickel–titanium alloy was used as the material for the implants in this paper, with conductivity and relative permittivity of 2.38×10^6 S/m and 1. The above completes the modeling of various human body postures, heart organs, and the metal coronary stent implant.

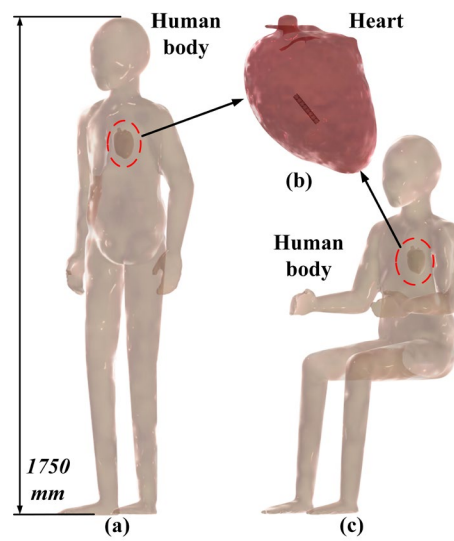


Figure 3. Human and organ models with a coronary stent implant. (a) Standing human model. (b) Heart model. (c) Sitting human model.

Table 1. Electromagnetic properties of human tissues at a frequency of 85 kHz.

	σ (s/m)	ϵ_r
Skin	0.20	1121
Fat	0.025	79
Muscle	0.27	5400
Bone	0.02	234
Lung	0.1	2888
Heart	0.21	11,137

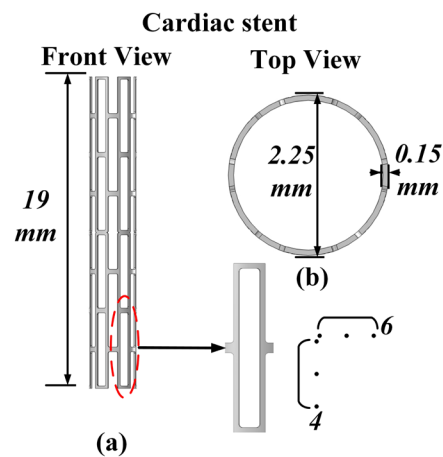


Figure 4. Coronary stent model. (a) Front view. (b) Top view.

2.3. Calculation Method

When analyzing the numerical calculation of electromagnetic fields, the MQS approach is used to calculate the values of electromagnetic fields when the wavelength of electromagnetic waves in space is larger than the geometry of the target to be solved. The approximation conditions for using the MQS approach are as follows:

$$|\alpha^2|d^2 \ll 1 \tag{8}$$

$$\alpha^2 = \omega(\omega\epsilon_r + j\sigma)\mu_0 \quad (9)$$

where α is the dielectric constant of the medium. In a lossless situation, the relationship between α and wavelength λ is $\alpha = 2\pi/\lambda$, ω is the angular frequency of the electromagnetic field, ϵ_r and σ are the permittivity and conductivity of human body tissues, μ_0 is the vacuum permeability with a value of $4\pi \times 10^{-7}$ (H/m), and d is the diameter of the computational region.

The MQS approach means that the rate of change of the displacement current $\partial D/\partial t$ can be neglected in Maxwell's equations, and the magnetic field can be treated as a steady-state magnetic field. The basic equations of the MQS approach are as follows:

$$\nabla \times \mathbf{H} = \mathbf{J} \quad (10)$$

$$\nabla \times \mathbf{E} = -\frac{\partial \mathbf{B}}{\partial t} \quad (11)$$

$$\nabla \cdot \mathbf{B} = 0 \quad (12)$$

$$\nabla \cdot \mathbf{D} = \rho \quad (13)$$

$$\mathbf{E} + \frac{\partial \mathbf{A}}{\partial t} = -\nabla \varphi \quad (14)$$

$$\mathbf{B} = \nabla \times \mathbf{A} \quad (15)$$

$$\nabla^2 \varphi = -\frac{\rho}{\epsilon} \quad (16)$$

$$\nabla^2 \mathbf{A} = -\mu \mathbf{J} \quad (17)$$

where \mathbf{H} is the magnetic field strength, \mathbf{J} is the current density, \mathbf{E} is the electric field strength, \mathbf{B} is the magnetic induction strength, \mathbf{D} is the potential shift vector, ρ is the charge volume density, ϵ is the dielectric constant of the medium, μ is the magnetic permittivity of the medium, and σ is the electrical conductivity of the medium. The medium relation of the field is $\mathbf{D} = \epsilon \mathbf{E}$, $\mathbf{B} = \mu \mathbf{H}$, and $\mathbf{J} = \sigma \mathbf{E}$. The magnetic potential is \mathbf{A} , and the scalar potential is φ . \mathbf{A} with respect to \mathbf{B} and \mathbf{E} and the coulomb gauge are introduced in Equations (10)–(13) to facilitate the calculation of the leakage EMF that needs to be solved in this paper.

In this paper, the transmission frequency of the EV-WPT device is 85 kHz, and the wavelength of electromagnetic waves in free space is of the order of several tens of meters. The size of the solution target is much smaller than the wavelength of electromagnetic waves when analyzing the EMF at this frequency [28]. Therefore, in this paper, the MQS approach in the electromagnetic field solver of the Comsol multi-physics field finite element simulation software version 6.1 is used to evaluate the electromagnetic exposure indices of humans with coronary stent implants under the EMF leaked from the EV-WPT device. The MQS approach calculates the internal human electromagnetic exposure index (the induced E -field value and SAR value) in two steps. This study is at a frequency of 85 kHz, so the main internal human electromagnetic exposure index studied is the induced E -field. In the first step, an equivalent current is taken at the surface of the WPT device, and then a non-uniform EMF identical to the original source is generated in the free space outside the surface according to the equivalence principle, and this non-uniform EMF is solved by introducing the magnetic vector potential in Equations (14) and (15). The non-uniform field obtained in the first step is considered as the field entering the body in the second step. Then, the electromagnetic exposure index inside the human body is solved by Maxwell's group and the time-domain finite difference method.

In solving the human body internal EMF index, it is known from the ICNIRP guidelines that when the human body is located in the EV-WPT device-leaked EMF at a frequency of 85 kHz, the index for quantitative assessment of human electromagnetic safety is the

human body's induced E -field, and based on ICNIRP, it is recommended that the human body's induced E -field is obtained using a continuous human body with a resolution of $2 \times 2 \times 2 \text{ mm}^3$. Therefore, in this paper, a resolution of $1 \times 1 \times 1 \text{ mm}^3$ is used to mesh the human body, which is in accordance with ICNIRP's recommendation for calculating the induced E -field value of the human body. Considering the more precise geometry of the implant and the larger induced E -field value of the human in the vicinity of the precise tip and sharp edge implant under the EMF, a resolution of $0.05 \times 0.05 \times 0.05 \text{ mm}^3$ is used to mesh the implant in order to obtain numerical calculation results with higher accuracy.

Considering the above numerical simulation calculation requirements, this paper uses Comsol multi-physics field finite element simulation software to quantify the electromagnetic exposure of humans with medical implants under the leaked EMF of the EV-WPT device. In order to quantify the effect of the WPT device misalignments generated in operation on the electromagnetic exposure of humans with medical implants, it is necessary to perform multiple batch calculations. The Comsol sweep function is used to calculate and evaluate the electromagnetic exposure of humans with medical implants in the case of the misalignments of WPT devices.

3. Numerical Simulation Calculation and Discussion

The above established numerical simulation model of human electromagnetism includes a coronary stent implant in the electromagnetic exposure scenario of an EV-WPT device, at a transmission frequency of 85 kHz and transmission powers of 11 kW and 22 kW. When the WPT device coils x_0 and z_0 have no misalignment and misalignments of 75 mm, the obtained 11 kW and 22 kW EV-WPT devices in the plane of the main visual cross-section E -field and magnetic flux density distributions are as shown in Figures 5 and 6. The figures show that the EV-WPT device generates a very uneven E -field and magnetic flux density between TC and RC and also in the surrounding space, and due to the shielding effect of the vehicle body, the E -field intensity inside the vehicle is much smaller than that outside the vehicle. But numerically, the maximum values of the E -field in the 11 kW and 22 kW spaces are 332.1 V/m and 234.5 V/m, respectively, which are much higher than the 83 V/m of the ICNIRP reference level. By comparison, it is found that when the WPT device is misaligned, the leakage E -field and magnetic flux density are generated with an uneven intensity distribution in the room, while the exposed E -field generated by the EV-WPT device is significantly enhanced at higher power levels, so it is necessary to quantitatively evaluate the induced E -field of the human body containing coronary stents exposed to this condition.

According to ICNIRP guidelines, the safety limit for the induced E -field value of the human body at a transmission frequency of 85 kHz is 11.475 V/m. It is not appropriate to use the 99th percentile as a result of this numerical calculation of the induced E -field value of the human body with medical implants because the 99th percentile value is not appropriate for quantifying the induced E -field value of the human body with implants. When quantifying the induced E -field value of the human body with an implant, the values are more widely distributed in the vicinity of human tissues around the implant, and taking the 99th percentile value and ignoring the top 1% may underestimate the true exposure; so, in situ values are used to quantify the calculated results to reflect the true exposure of human tissues near the sharp edges of the implant.

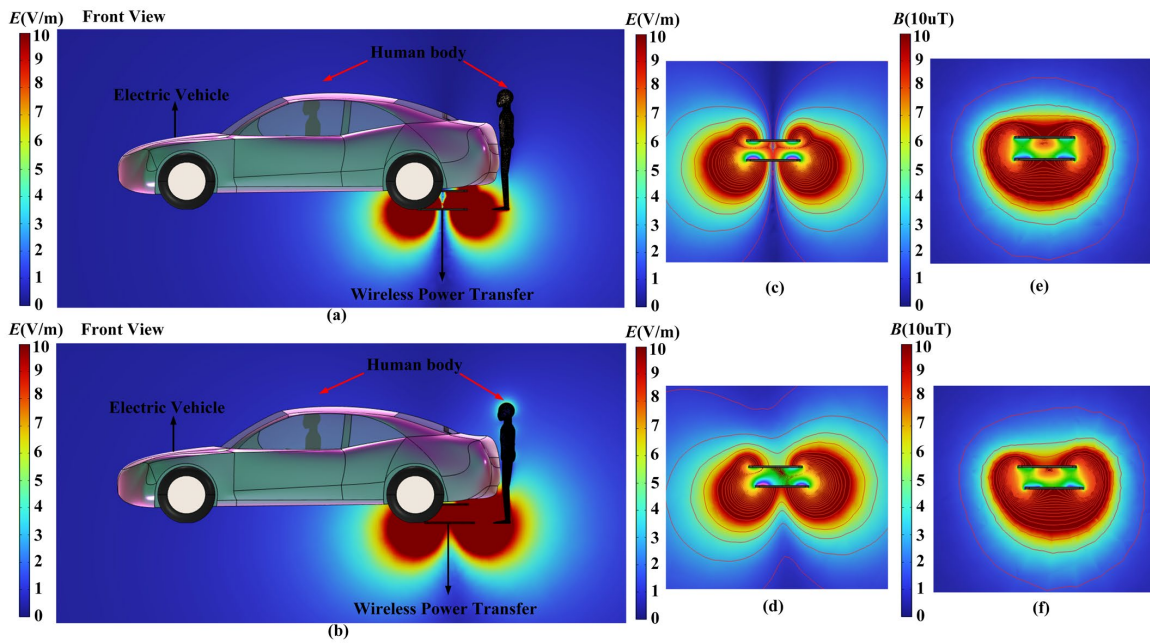


Figure 5. The field spatial distribution of the EV-WPT device with the transmission power of 11 kW in the main cross-sectional plane. (a) The E -field of normal operation of the EV-WPT device. (b) The E -field of misalignments in operation of the EV-WPT device. (c) The E -field of normal operation of the WPT without the human and car. (d) The E -field of misalignments in operation of the WPT without the human and car. (e) The magnetic flux density of normal operation of the WPT without the human and car. (f) The magnetic flux density of misalignments in operation of the WPT without the human and car.

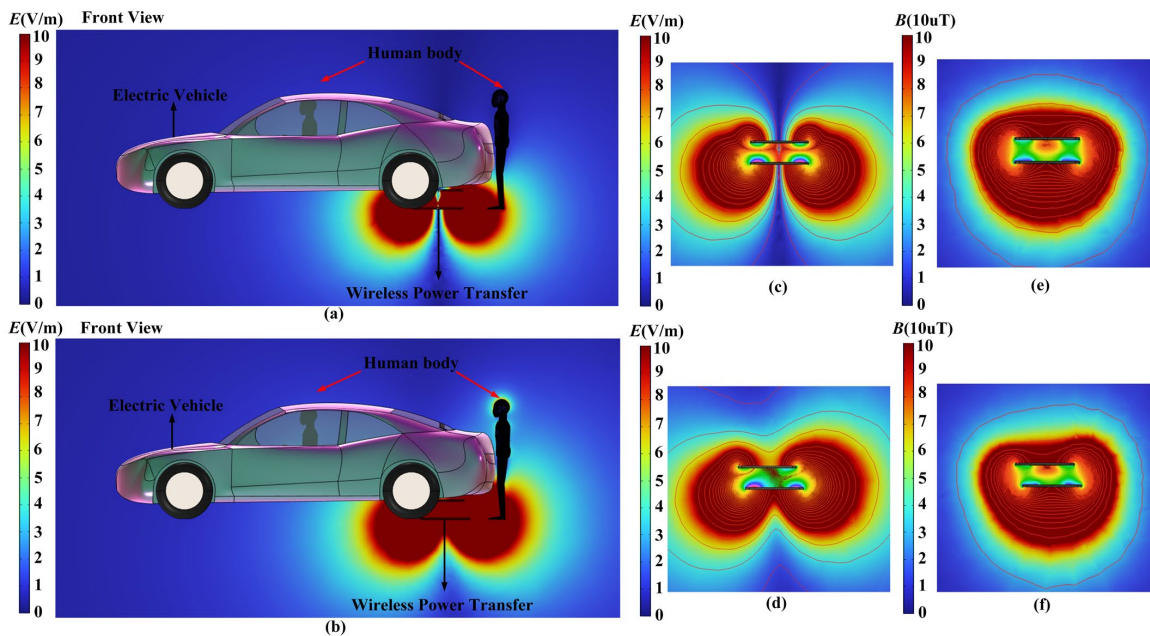


Figure 6. The field spatial distribution of the EV-WPT device with the transmission power of 22 kW in the main cross-sectional plane. (a) The E -field of normal operation of the EV-WPT device. (b) The E -field of misalignments in operation of the EV-WPT device. (c) The E -field of normal operation of the WPT without the human and car. (d) The E -field of misalignments in operation of the WPT without the human and car. (e) The magnetic flux density of normal operation of the WPT without the human and car. (f) The magnetic flux density of misalignments in operation of the WPT without the human and car.

The standing human body is located at the rear of the vehicle, and the sitting human body is located in the driver's position. There is no bit error in the x_0 and z_0 of the coil of the WPT device, the induced E -field distributions of the standing human body under the WPT device with transmission powers of 11 kW and 22 kW are shown in Figures 7 and 8, and the induced E -field distributions of the sitting human body under the WPT device with transmission powers of 11 kW and 22 kW are shown in Figures 9 and 10. As shown in Figures 9 and 10, comparative numerical simulations are performed using the same grids for different electromagnetic exposure scenarios: a human body without implants and a human body with implants. According to the numerical simulation, the coronary stent implant has a significant effect on the distribution of the E -field in human tissues in different postures. The induced E -field of human tissues near the sharp edges of the implants is significantly larger than that of the body without implants. The larger values of the induced E -field are distributed at both ends of the coronary stents. Wave diffraction may be the mechanism that causes a significant enhancement of the induced E -field around the sharp edges and tips of implants. The presence of metallic implants in vivo causes scattering of incident electromagnetic waves, and sharp edges have the potential for high electromagnetic energy dissipation, which alters the spatial distribution of the electric field. Thus, the coronary stent implant significantly affects the induced E -field in the human heart, especially around the sharp edges of the coronary stent implant. According to Figures 7–10, the induced E -field distribution near the apical edge of the implant is significantly enhanced regardless of the posture of the human body compared to the induced E -field distribution of the coronary stent implant in other regions of the human body, and the maximum values of the cardiac induced E -field values are distributed at the sharp ends of the coronary stent implant. As shown in Table 2, the cardiac induced E -field_{max} values are also greatly enhanced when a coronary stent is implanted in the body. Comparison of the induced E -field_{max} value of the human body in Table 2 shows that the higher the power of the nonimplanted WPT device, the higher the induced E -field_{max} value of the human body, and the induced E -field_{max} value of the human body with an implanted coronary stent is significantly enhanced compared to that of the nonimplanted one. The induced E -field_{max} value of the human body with an implant for a WPT device with a transmission power of 22 kW is 1.758 V/m, which is well below the safe limit. Still, when the WPT device is misaligned, it generates a relatively large leakage of EMFs in space, and the value may exceed the limit, which causes the induced E -field value of the human heart tissue with a coronary stent implant to exceed the safety limit, and there may be a potential safety hazard of EMR to the human heart organ. So, it is necessary to quantify the misalignment situation.

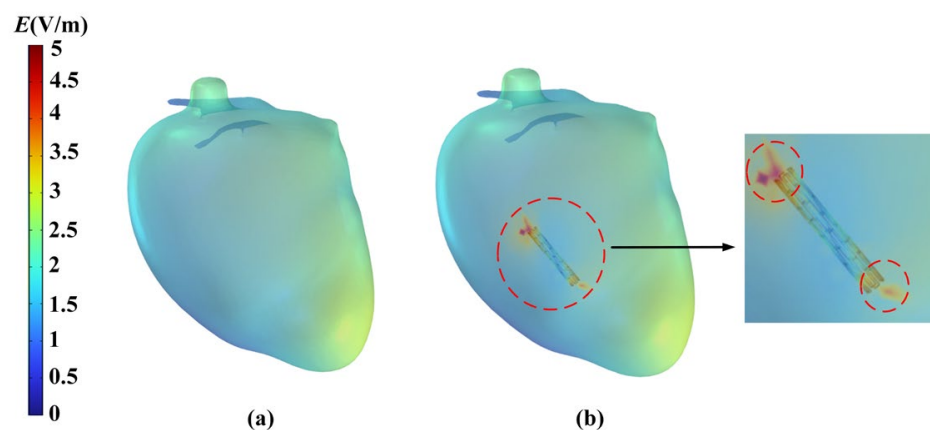


Figure 7. The induced E -field distribution of the human with a coronary stent implant. (a) WPT device with the transmission power of 11 kW and human standing without the implant. (b) WPT device with the transmission power of 11 kW and human standing with the implant.

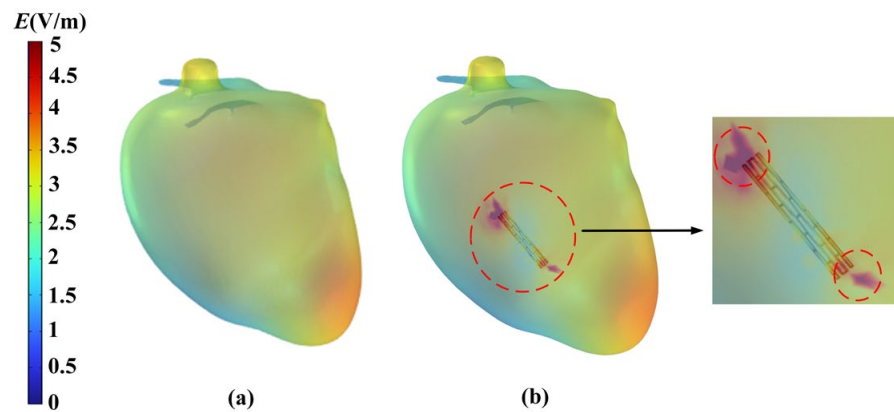


Figure 8. The induced E -field distribution of the human with a coronary stent implant. (a) WPT device with the transmission power of 22 kW and human sitting without the implant. (b) WPT device with the transmission power of 22 kW and human standing with the implant.

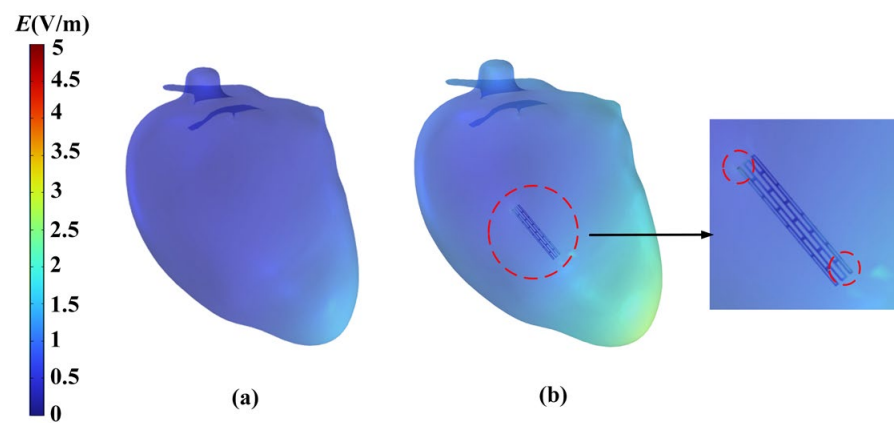


Figure 9. The induced E -field distribution of the human with a coronary stent implant. (a) WPT device with the transmission power of 11 kW and human sitting without the implant. (b) WPT device with the transmission power of 11 kW and human sitting with the implant.

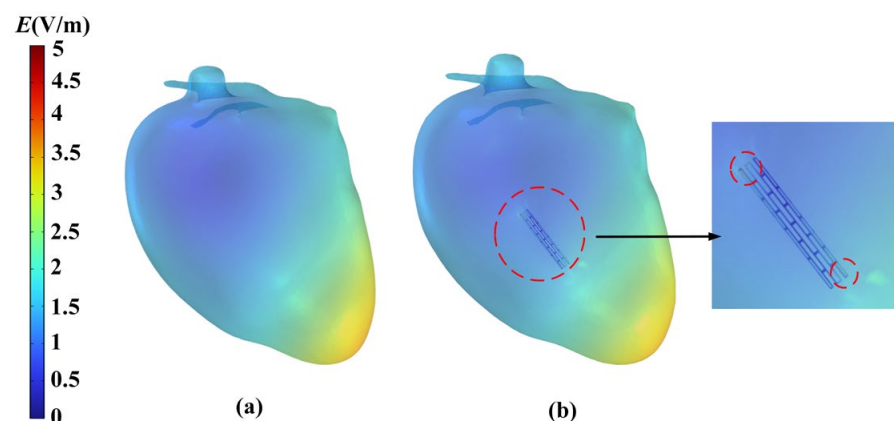


Figure 10. The induced E -field distribution of the human with a coronary stent implant. (a) WPT device with the transmission power of 22 kW and human sitting without the implant. (b) WPT device with the transmission power of 22 kW and human sitting with the implant.

Table 2. Results of induced $E\text{-field}_{\max}$ in the humans with different postures containing a coronary stent in the absence of misalignments generated in WPT devices of different powers.

WPT Device Power/Body Posture	Induced $E\text{-field}_{\max}$ for Humans without Implants (V/m)	Induced $E\text{-field}_{\max}$ for Humans with Implants (V/m)
11 kW/human sitting	0.027	0.677
11 kW/human standing	0.061	1.292
22 kW/human sitting	0.037	0.989
22 kW/human standing	0.083	1.758

In order to obtain the effect of generated EV-WPT device misalignments on the electromagnetic exposure of a human body containing medical implants, considering the EV-WPT device in operation, we must consider that the driver's parking operation allows for the WPT device coil to be out of alignment, so there is a certain amount of misalignments generated; and the reference standard sets the range of variation in misalignments x_0 and z_0 of the WPT device coil in 2.1 to be $[-75 \text{ mm}, 75 \text{ mm}]$ [22], with a sweep parameter step size of 15 mm, which are calculated for comparison of the induced $E\text{-field}_{\max}$ value of a human body without implants and with a coronary stent, respectively. The results of the induced $E\text{-field}_{\max}$ value of the human body without implants and with a coronary stent in different postures under the leaked EMF of the EV-WPT device with different powers are shown in Figures 11–14. According to the Figures, when the sitting human body without an implant is in the driving position and the standing human body is at the rear of the vehicle, when the WPT device generates misalignments, the maximum values of the induced $E\text{-field}_{\max}$ value of the human body are 0.039 V/m and 0.091 V/m, respectively, at a transmission power of 11 kW. The maximum values of the induced $E\text{-field}_{\max}$ value of the human body are 0.050 V/m and 0.124 V/m, respectively, at a transmission power of 22 kW. The numerical value does not exceed the ICNIRP safety limit. Still, the obtained results of the induced $E\text{-field}_{\max}$ are not symmetrically distributed with the misalignments generated because the human body in different postures is not directly above the WPT device, and the degree of influence of the misalignments in the x - and z -directions is inconsistent when the misalignments are generated. For a human body containing a coronary stent implant and a WPT device generating misalignments, the induced $E\text{-field}_{\max}$ values for a sitting human body exposed to a WPT device with transmission powers of 11 kW and 22 kW are 3.087 V/m and 5.790 V/m, respectively, neither of which exceeds the ICNIRP safety limit, partly because of the weak EMFs within the shielding effect of the EV body and partly because the human body is further away from the WPT device and receives weaker electromagnetic energy. However, the induced $E\text{-field}_{\max}$ of the standing human body under the WPT device with the transmission power of 11 kW will exceed the ICNIRP safety limit in 8.3% of the misalignment range in the case of misalignments, with the maximum value of 11.839 V/m, which is 103.2% of the ICNIRP safety limit. The induced $E\text{-field}_{\max}$ of the standing human body under the WPT device with the transmission power of 22 kW will also exceed the ICNIRP safety limit when the misalignments are small; 46.4% of the range of misalignments will exceed the ICNIRP safety limit value; the maximum value is 17.242 V/m, 150.3% of the ICNIRP safety limit value; and generally, the calculation results of the human body in the standing position are more significant than those in the sitting position. This is because the WPT device is located at the rear of the vehicle, and the closer the relative distance between the human body and the WPT device, the larger the leaked EMF is. The reason is that the WPT device is located at the rear of the vehicle, and the closer the human body is to the WPT device, the greater the leakage of EMFs and the greater the induced $E\text{-field}_{\max}$ of the human body. When the human body is implanted with a coronary implant, the WPT misalignments generated have a more significant effect on the human body's induced $E\text{-field}_{\max}$ value. The human body in the standing position has a different degree of exceeding the ICNIRP safety limit; the greater the power, the greater the misalignment distance, and the greater the degree of exceeding the limit. In addition, the

coronary stent implant has a significant influence on the distribution of the induced E -field in the human body. From the perspective of the geometry of the implant, the coronary stent has sharper edges, which have a higher electromagnetic energy dissipation capacity, and the surrounding human body tissues have a higher energy absorption capacity.

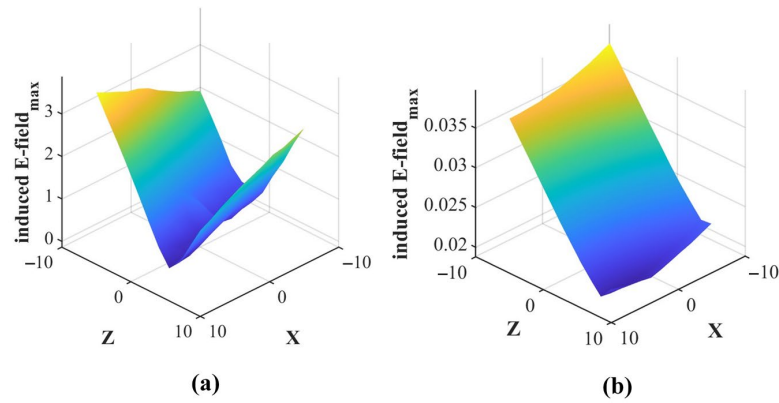


Figure 11. Sweep parameter plots of induced E -field_{max} for sitting human body under EV-WPT device with the transmission power of 11 kW: (a) human body with implant; (b) human body without implant.

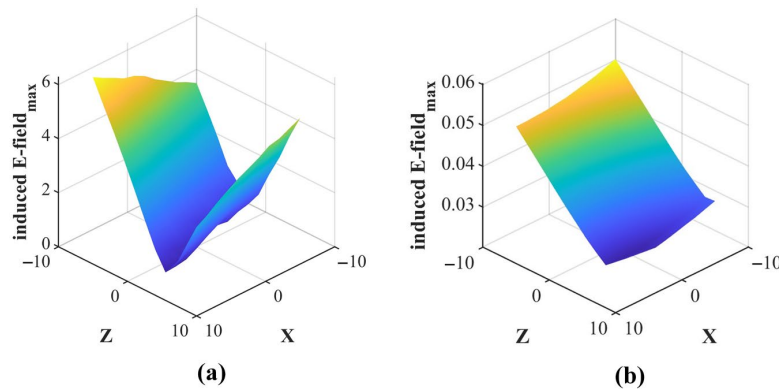


Figure 12. Sweep parameter plots of induced E -field_{max} for sitting human body under EV-WPT device with the transmission power of 22 kW: (a) human body with implant; (b) human body without implant.

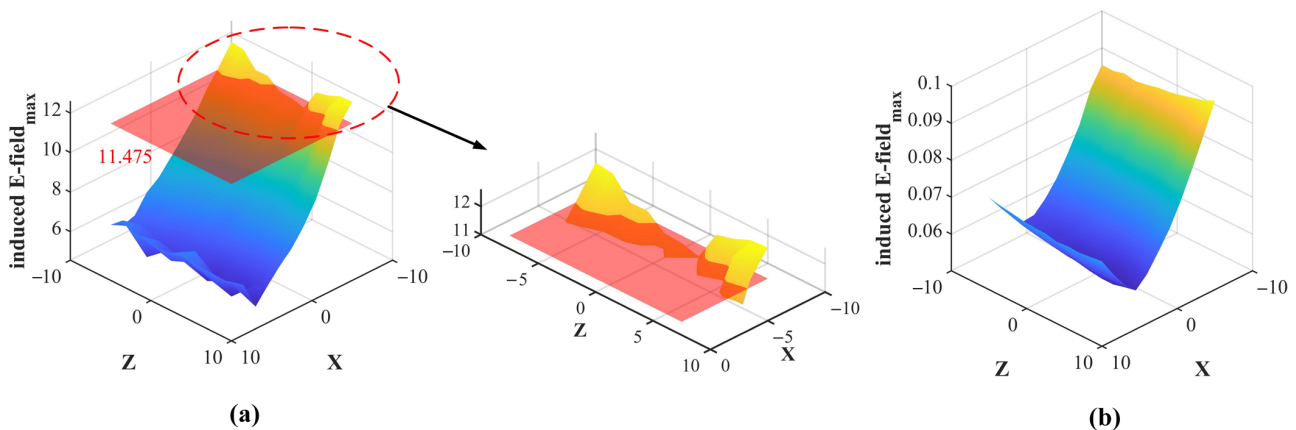


Figure 13. Sweep parameter plots of induced E -field_{max} for standing human body under EV-WPT device with the transmission power of 11 kW: (a) human body with implant; (b) human body without implant.

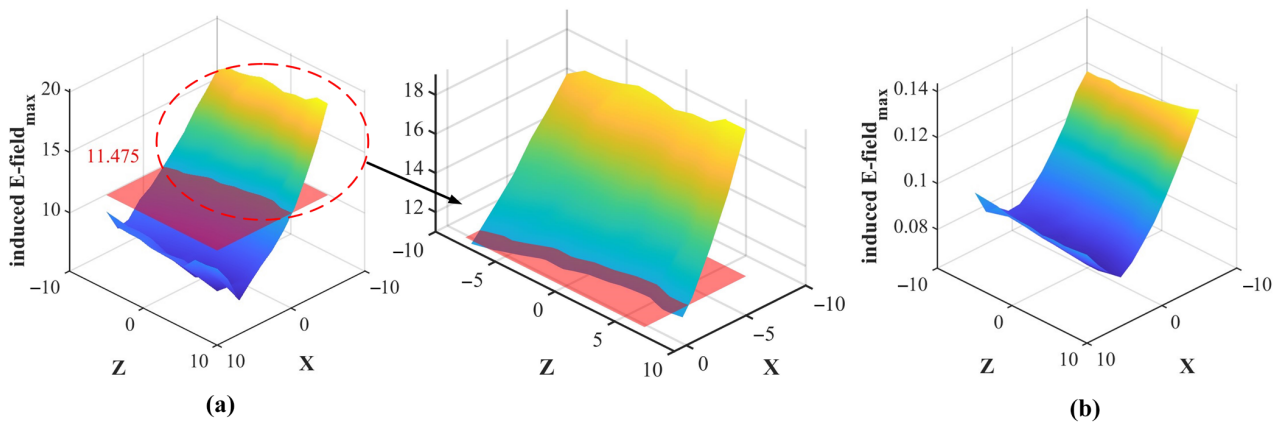


Figure 14. Sweep parameter plots of induced $E\text{-field}_{\max}$ for standing human body under EV-WPT device with the transmission power of 22 kW: (a) human body with implant; (b) human body without implant.

By analyzing and discussing the results of the numerical simulation calculations, it can be concluded that the main factors affecting the value of the induced $E\text{-field}_{\max}$ in the human body are the degree of the WPT device misalignments generated, the structural shape of the implant, the relative position of the human body containing the implant and the WPT device, and the power of the WPT device. Therefore, in order to ensure the electromagnetic safety of the human body containing medical implants under the high-power EV-WPT device, attention should be paid to the misalignments of the WPT device to try to ensure that it operates in a non-misalignment situation and the relative position of the human body to the WPT device should be ensured to be in a safe range when charging the EV-WPT device, as well as strengthening related research on the optimal design of the leaked EMF shielding of the WPT device.

4. Conclusions

This paper aims to quantitatively assess the electromagnetic exposure of human subjects with coronary stent implants when the EV-WPT device generates misalignments. The quantification of the induced $E\text{-field}$ in the human body is performed considering different power levels and different postures of the human body at a transmission frequency of 85 kHz when the charging operation of the WPT device generates different degrees of misalignments. The results show that coronary stents have a significant effect on the internal $E\text{-field}$ strength of the human body, and the induced $E\text{-field}$ of the human tissues around an implant is significantly enhanced compared to that without an implant at the same power and in the same body posture. The induced $E\text{-field}$ value of the human body near the edge of the implant tip is greater. At the same time, the WPT device misalignments generated have a greater impact on human electromagnetic exposure. In the case of $[-7.5\text{ mm}, 7.5\text{ mm}]$ misalignments, at a transmission power of 11 kW and with the human body in a standing position, 8.3% of the misalignment cases will lead to the human body's induced $E\text{-field}_{\max}$ exceeding the safety limit, of which the maximum exceeds the limit of 3.2%; at a transmission power of 22 kW with the human body in a standing position, 46.4% of misalignment cases will cause the human body's induced $E\text{-field}$ to exceed the safety limit, of which the maximum value exceeds the limit by 50.3%. In addition, the transmission power of the WPT device and the distance between the human body and the WPT device have a corresponding effect, with higher EV-WPT transmit power and closer proximity between the human body and the WPT device leading to higher values of the induced $E\text{-field}$ in the human body with a coronary stent implant. In order to ensure the relative safety of the human body with a coronary stent implant, it is necessary to ensure that the transmission power of the EV-WPT device is below 11 kW. Moreover, when charging the high-power EV-WPT device, there is a potential electromagnetic safety problem for the

human body with a coronary stent implant. Attention should be paid to the misaligned operation of the WPT device to avoid the misaligned operation and ensure that the human is in a relatively safe position when charging. At the same time, research on the optimal design of the electromagnetic shielding of the WPT device should be strengthened.

Author Contributions: Conceptualization, T.W., B.L., and S.G.; methodology, T.W.; software, B.L.; validation, T.W., B.L., and K.Z.; formal analysis, T.W.; investigation, T.W.; resources, Q.Y.; data curation, T.W., B.L., and S.G.; writing—original draft preparation, T.W., B.L., and K.Z.; writing—review and editing, T.W. and S.G.; visualization, Q.Y. and S.G.; supervision, L.X.; project administration, T.W. and Y.C.; funding acquisition, T.W. All authors have read and agreed to the published version of the manuscript.

Funding: This research was funded by the Jilin Scientific and Technological Development Program (grant numbers 20230201122GX and 20220101196JC) and by the Key Laboratory for Comprehensive Energy Saving of Cold Regions Architecture of the Ministry of Education, Jilin Jianzhu University (grant number JljzhdKF202203).

Data Availability Statement: The data that support the findings of this study are available from the corresponding author upon reasonable request.

Conflicts of Interest: The authors declare no conflict of interest.

References

1. Mi, C.C.; Buja, G.; Choi, S.Y.; Rim, C.T. Modern advances in wireless power transfer systems for roadway powered electric vehicles. *IEEE Trans. Ind. Electron.* **2016**, *31*, 6533–6545. [[CrossRef](#)]
2. Zhang, Z.; Pang, H.L.; Georgiadis, A.; Cecati, C. Wireless power transfer—An overview. *IEEE Trans. Ind. Electron.* **2019**, *66*, 1044–1058. [[CrossRef](#)]
3. Campi, T.; Cruciani, S.; Maradei, F.; Feliziani, M. Near-Field Reduction in a Wireless Power Transfer System Using LCC Compensation. *IEEE Trans. Electromagn. Compat.* **2017**, *59*, 686–694. [[CrossRef](#)]
4. Luo, Z.; Zhao, Y.; Xiong, M.; Wei, X.; Dai, H. A Self-Tuning LCC/LCC System Based on Switch-Controlled Capacitors for Constant-Power Wireless Electric Vehicle Charging. *IEEE Trans. Ind. Electron.* **2023**, *70*, 709–720. [[CrossRef](#)]
5. Daga, A.; Miller, J.M.; Long, B.R.; Kacergis, R.; Schrafel, P.; Wolgemuth, J. Electric Fuel Pumps for Wireless Power Transfer: Enabling rapid growth in the electric vehicle market. *IEEE Power Electron. Mag.* **2017**, *4*, 24–35. [[CrossRef](#)]
6. Yu, Q.; Lin, J.; Ma, X.; Li, B.; Xu, L.; Wang, T. Efficiency Optimization of Wireless Power Transfer System for Electric Vehicle Based on Improved Marine Predators Algorithm. *IEEE Trans. Intell. Transp. Syst.* **2023**, *24*, 7847–7858. [[CrossRef](#)]
7. Geng, Y.; Guo, Q.; Yang, Z.; Lin, F.; Wang, Y. Design and Optimization of Real-time Strong Coupling Coil of Dynamic Wireless Power Transfer for Electrical Vehicle. *IEEE Trans. Veh. Technol.* **2023**, *72*, 11495–11504. [[CrossRef](#)]
8. Brovont, A.D.; Aliprantis, D.; Pekarek, S.D.; Vickers, C.J.; Mehar, V. Magnetic Design for Three-Phase Dynamic Wireless Power Transfer with Constant Output Power. *IEEE Trans. Energy Convers.* **2023**, *38*, 1481–1484. [[CrossRef](#)]
9. Wang, Q.; Li, W.; Kang, J.; Wang, Y. Electromagnetic safety of magnetic resonant wireless charging system in electric vehicles. In Proceedings of the IEEE PELS Workshop on Emerging Technologies, Chongqing, China, 20–22 May 2017.
10. Laakso, I.; Hirata, A. Evaluation of the induced electric field and compliance procedure for a wireless power transfer system in an electrical vehicle. *Phys. Med. Biol.* **2013**, *58*, 7583–7593. [[CrossRef](#)]
11. International Commission on Non-Ionizing Radiation Protection (ICNIRP). Guidelines for limiting exposure to time-varying electric and magnetic fields (1 Hz to 100 kHz). *Health Phys.* **2010**, *99*, 818–836. [[CrossRef](#)]
12. International Commission on Non-Ionizing Radiation Protection (ICNIRP). Guidelines for limiting exposure to time-varying electric and magnetic fields (100 kHz to 300 GHz). *Health Phys.* **2020**, *118*, 483–524. [[CrossRef](#)]
13. Mumtaz, S.; Rana, J.N.; Choi, E.H.; Han, I. Microwave Radiation and the Brain: Mechanisms, Current Status, and Future Prospects. *Int. J. Mol. Sci.* **2022**, *23*, 9288. [[CrossRef](#)] [[PubMed](#)]
14. Shimamoto, T.; Laakso, I.; Hirata, A. In-situ electric field in human body model in different postures for wireless power transfer system in an electrical vehicle. *Phys. Med. Biol.* **2015**, *60*, 163–173. [[CrossRef](#)] [[PubMed](#)]
15. Park, S. Evaluation of Electromagnetic Exposure During 85 kHz Wireless Power Transfer for Electric Vehicles. *IEEE Trans. Magn.* **2018**, *54*, 1–8. [[CrossRef](#)]
16. Perpétuo, L.; Barros, A.S.; Dalsuco, J.; Nogueira-Ferreira, R.; Resende-Gonçalves, P.; Falcão-Pires, I.; Ferreira, R.; Leite-Moreira, A.; Trindade, F.; Vitorino, R. Coronary Artery Disease and Aortic Valve Stenosis: A Urine Proteomics Study. *Int. J. Mol. Sci.* **2022**, *23*, 13579. [[CrossRef](#)]
17. Lan, Y.; Zhou, Y.; Lu, Y.; Wang, H.; Liu, Q.; Ng, E.Y.K.; Peng, Y.; Hao, Y.; Liu, Q.; Chen, F.; et al. A Nine Months Follow-up Study of Hemodynamic Effect on Bioabsorbable Coronary Stent Implantation. *IEEE Access* **2019**, *7*, 112564–112571. [[CrossRef](#)]
18. Li, D.; Zheng, J.; Liu, Y.; Pan, C.; Kainz, W.; Yang, F.; Wu, W.; Chen, J. An Efficient Approach to Estimate MRI RF Field Induced In Vivo Heating for Small Medical Implants. *IEEE Trans. Electromagn. Compat.* **2015**, *57*, 643–650. [[CrossRef](#)]

19. Iqbal, A.; Al-Hasan, M.; Mabrouk, I.B.; Basir, A.; Nedil, M.; Yoo, H. Biotelemetry and Wireless Powering of Biomedical Implants Using a Rectifier Integrated Self-Diplexing Implantable Antenna. *IEEE Trans. Microw. Theory Tech.* **2021**, *69*, 3438–3451. [[CrossRef](#)]
20. Shah, I.A.; Basir, A.; Cho, Y.; Yoo, H. Safety Analysis of Medical Implants in the Human Head Exposed to a Wireless Power Transfer System. *IEEE Trans. Electromagn. Compat.* **2022**, *64*, 640–649. [[CrossRef](#)]
21. Shah, I.A.; Yoo, H. Assessing Human Exposure with Medical Implants to Electromagnetic Fields from a Wireless Power Transmission System in an Electric Vehicle. *IEEE Trans. Electromagn. Compat.* **2020**, *62*, 338–345. [[CrossRef](#)]
22. Wireless Power Transfer for Light-Duty Plug-In/Electric Vehicles and Alignment Methodology, International Standard SAE J2954. 2019. Available online: https://www.sae.org/standards/content/j2954_201904/ (accessed on 28 May 2023).
23. Campi, T.; Cruciani, S.; Maradei, F.; Feliziani, M. Magnetic Field during Wireless Charging in an Electric Vehicle According to Standard SAE J2954. *Energies* **2019**, *12*, 1795. [[CrossRef](#)]
24. Kan, T.; Nguyen, T.D.; White, J.C.; Malhan, R.K.; Mi, C.C. A New Integration Method for an Electric Vehicle Wireless Charging System Using LCC Compensation Topology: Analysis and Design. *IEEE Trans. Power Electron.* **2017**, *32*, 1638–1650. [[CrossRef](#)]
25. Bevacqua, M.T.; Bellizzi, G.G.; Crocco, L.; Isernia, T. A method for quantitative imaging of electrical properties of human tissues from only amplitude electromagnetic data. *Inverse Probl.* **2019**, *35*, 025006. [[CrossRef](#)]
26. Wang, T.; Yu, Q.; Li, B.; Lv, G.; Wu, Y.; Guan, S. Uncertainty Quantification of Human Electromagnetic Exposure from Electric Vehicle Wireless Power Transfer System. *IEEE Trans. Intell. Transp. Syst.* **2023**, *24*, 8886–8896. [[CrossRef](#)]
27. Wang, W.; Poh, C.K. Titanium alloys in orthopaedics. In *Titanium Alloys: Advances in Properties Control*; InTech: Rijeka, Croatia, 2013.
28. Christ, A.; Douglas, M.; Nadakuduti, J.; Kuster, N. Assessing Human Exposure to Electromagnetic Fields from Wireless Power Transmission Systems. *Proc. IEEE* **2013**, *101*, 1482–1493. [[CrossRef](#)]

Disclaimer/Publisher’s Note: The statements, opinions and data contained in all publications are solely those of the individual author(s) and contributor(s) and not of MDPI and/or the editor(s). MDPI and/or the editor(s) disclaim responsibility for any injury to people or property resulting from any ideas, methods, instructions or products referred to in the content.